Al-Qadisiyah Journal of Pure Science

Volume 29 | Number 2 Article 23

12-20-2024

Synthesis, characterization, and biological assay of Ni(II), Pd(II), and Pt(IV) complexes based on tridentate imidazole ligand

Howraa Saad Abd Alwahid
Ministry of Education, Directorate of Education Al-Qadisiyah, Al Diwaniyah, Iraq.

Khalid J. Al-Adilee
Department of Chemistry, College of Science, University of Al-Qadisiyah, Diwaniya 1753, Iraq,
khalid.jawad@qu.edu.iq

Recommended Citation

Alwahid, Howraa Saad Abd and Al-Adilee, Khalid J. (2024) "Synthesis, characterization, and biological assay of Ni(II), Pd(II), and Pt(IV) complexes based on tridentate imidazole ligand," *Al-Qadisiyah Journal of Pure Science*: Vol. 29 : No. 2 , Article 23.
Available at: https://doi.org/10.29350/2411-3514.1305

ORIGINAL STUDY

Synthesis, Characterization, and Biological Assay of Ni(II), Pd(II), and Pt(IV) Complexes Based on Tridentate Imidazole Ligand

Howraa S.A. Alwahid [a,*], Khalid J. Al-Adilee [b]

[a] Ministry of Education, Directorate of Education Al-Qadisiyah, Al Diwaniyah, Iraq
[b] Department of Chemistry, College of Science, University of Al-Qadisiyah, Diwaniya 1753, Iraq

Abstract

Three new mononuclear metal complexes of the type ML(M = Ni, Pd, and Pt), with (N,N,O) azo ligand, 2-[2'-(3,4-Dimethyl carboxy phenyl)azo]-4,5-Dichloro imidazole (L_1H), have been prepared and characterized using Uv-vis., FT-IR, NMR and elemental (C.H.N) analyses. In addition, all complexes were analyzed by molar conductance, magnetic susceptibility, and thermogravimetric analyses. The spectroscopic techniques showed that the ligand under investigation behaves as a tridentate ligand (N,N,O). Further, the free radical scavenging activity of ligand and metal complexes have been determined by their interaction with the stable DPPH free radical. All the compounds exhibited significant antiproliferative activity against the human breast cancer line, MCF-7, and normal cells HdFn. Results showed higher cytotoxic activity and lower IC_{50} values, suggesting they can kill cancer cells at very low concentrations.

Keywords: Antibacterial activity, DPPH, MCF-7, DFT, HOMO

1. Introduction

The imidazole nucleus plays a key role in biological activities as it mimics several important biological building blocks, including histidine (a constituent of most proteins), histamine, purines, and biotin, which play a key role in life. In many categories of therapeutic reagents, the imidazole nucleus is considered the "Master Key" because it is an important core component [1–3]. Among others, imidazole nucleus is used as an anti-cancer, antimicrobial, anti-inflammatory, anti-diabetic, antihypertensive, anti-tubercular, antiviral, antiparasitic, antiviral, antiparasitic reagents, anti-inflammatory, anti-inflammatory, anti-coagulant, anti-coagulant, hormone modulators, CNS stimulants, depressants, and lipid modulators [4–10].

Azo dyes were named with this name due to the presence of the azo bridge group with sp^2 hybridization associated with the aromatic system [11]. A group of two atoms called a bridge group is formed by these two atoms. They are called aliphatic azo dyes and they are less widely used due to their rapid disintegration into hydrocarbons and nitrogen. In terms of azo dyes aromatic, the azo group (-N=N-) links two aromatic groups (Ar-N=N-Ar) and this type is more important and widespread due to the high stability and multiple uses of these compounds [12,13]. On one hand, azobenzene [14] is the simplest example, but on the other, azo dyes differ in color depending on their composition and compensated groups. The intensity of color increases when the color-donating chromophores or the molecular weight increases, and the compensated groups affect the benzene ring carrying the chromophore group by increasing the color intensity. These groups are called exochromic groups [15,16].

In light of these observations, Ni(II), Pd(II), and Pt(IV) complexes were prepared and characterized

Received 26 February 2023; accepted 18 May 2023.
Available online 18 April 2025

* Corresponding author.
E-mail address: khalid.jawad@qu.edu.iq (H.S.A. Alwahid).

https://doi.org/10.29350/2411-3514.1305

by elemental analysis, molar conductance, spectral, and thermal analysis. The synthesized compounds were evaluated for their antioxidant properties. Moreover, we investigated the anticancer activities of ligand and Pd(II) complex.

2. Experimental

2.1. Materials and methods

Fluka, Sigma-Aldrich, Merck, Scharlu, J&K Chemical, BDH, and others supplied all starting materials to this study.

A variety of spectroscopic techniques were used to characterize the synthesized complexes. A Bruker Advance II 400 MHz spectrometer was used to obtain NMR spectra at ^{1}H & ^{13}C using DMSO-d6 as solvents with TMS used as a standard reference. Infrared spectra (KBr pellets; 400–4000 cm^{-1}) were recorded on a Perkin-Elmer 983 spectrophotometer. Using ethanol absolute at room temperature, the complex absorption spectra were measured on a Perkin-Elmer UV-Vis spectrophotometer. A Euro vector model EA/3000 was used to analyze the elements (C, H, and N). Metal ions were calculated gravimetrically as metal oxides. At 25 °C, the ligand and its complexes were measured using a conductometer WTW, at a concentration of 1×10^{-3} M. Johnson Mattey catalytic system division measured magnetic measurements at 25 °C. On a Shimadzu Agilent Technologies 5973C mass spectrometer (70 eV), mass spectra were recorded for both the ligand and the metal complexes. The thermal decomposition of compounds was studied using TGA and DTA (DTG-60H, Shimadzu TG-50). A decomposition apparatus was used to record the melting points of compounds and the data has not been corrected. The pH was measured with a Philips PW 9421 (±0.001). The X-ray diffraction measurements were conducted using an aluminum anode X-ray diffractometer of 2Θ (20–80°). ChemBioDraw Ultra 10.0 software was used to generate chemical names.

2.2. General synthesis of ligand and metal complexes

2.2.1. Synthesis of 2-[2'-(3,4-dimethyl carboxy phenyl)azo]-4,5-dichloro imidazole (L_1H)

According to the method described in the method of work, some modifications were made to the ligand (L_1H) prepared by Al-Adliee and his group [17–20] (Scheme 1). In the first step, 1.6 g (0.01 mol) of 2-amino-3,4-dimethyl benzoic acid was dissolved in 40 ml of distilled water with 5 ml of concentrated hydrochloric acid. After cooling the mixture at (0–3) ºC, a solution containing 0.7 g (0.01 mol) sodium nitrite dissolved in 35 mL of distilled water was added, with continuous stirring, ensuring that the temperature did not exceed 3 °C while cooling. In the second step, 1.37 g (0.01 mol) of 4,5-dichloroimidizol were dissolved in 30 mL of ethanol absolute, then 12 mL of sodium hydroxide (NaOH) 10 % was added, and finally, the mixture was cooled.

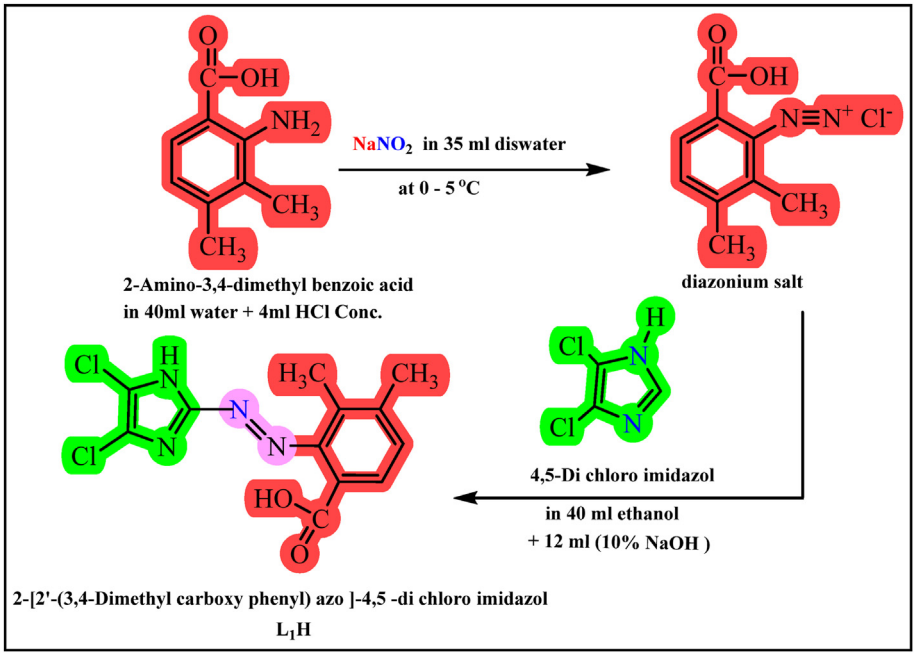

Scheme 1. Novel azo dye ligand synthesized.

Immediately after refluxing for 1 h and cooling to 0–5 °C. After filtering and collecting the precipitate, it was reconstituted. Several washes of distilled water were done on the precipitate, followed by recrystallization in ethanol and overnight drying at 60 °C. Color: yellow semi-crystals. Yield: 87 %. Melting point: 167 °C. MW: 327.17. pH: 6.5. Chemical Formula: $C_{13}H_{12}Cl_2N_4O_2$.

2.2.2. Synthesis of metal complexes

The preparation of metal complexes has been reported previously. Hot buffer solutions of nickel (II) chloride (0.237 g, 1.00×10^{-3} mol, 1:2 [M:L]), palladium(II) chloride (0.177 g, 1.00×10^{-3} mol, 1:1 [M:L]), (0.177 g, 1.00×10^{-3} mol, 1:1 [M:L]), chloroplatinic acid hexahydrate (0.327 g, 1.00×10^{-3} mol, 1:1 [M:L]) and the ligand (0.624 g in 30 mL ethanol) were refluxed for 2 h with constant magnetic stirring. Overnight, the mixture was evaporated. After filtering and washing with ethanol, the solid products were re-crystallized. Besides physical properties, Table 1 includes analytical data on C, H, and N.

2.3. Antiradical assay

A method previously described [21] was used to measure the DPPH radical scavenging activity of ligands and metal complexes. DMSO was used to dissolve ligand and metal complexes in concentrations (12.5, 25, 50, 100, and 200 μg/ml). After shaking these solutions vigorously with DPPH solution (0.2 mM in methanol), 2 ml of DPPH solution was added. After 30 min of incubation at 37 °C and in the dark, the mixture was cooled. Every 5 min, the absorbance of DPPH was measured at 517 nm. Control samples (2 ml) of DPPH were also tested at 517 nm. According to the following equation, free radical scavenging ratios can be calculated; Free radical scavenging ratio (%) = $[(A_1 - A_2)/(A_1)] \times 100$ %, where $[A_2]$ is the absorbance in the presence of ligand or a metal complex and $[A_1]$ is the absorbance of the blank [22].

2.4. Cytotoxicity (MTT assay)

Human breast cancer cells (MCF-7) and human dermal fibroblasts neonatal (HDFn) are cytotoxic to the ligand and Pd(II) metal complex in vitro. Using MTT assays (Microculture Tetrazolium Assays), selected synthetic compounds that are cytotoxic were identified [23]. For the experiment, cells were transferred into 96 wells (10^4 cells per well) for 24 h before being transmuted with metal imine chelates for adhesion to the plate walls at a density of 5×10^3 cells per well. Different concentrations of

Table 1. A description of the physical properties and analytical data for the free ligand and their metal complexes.

Compound	Color	m.p °C	pH	Yield %	Molecular Formula (M.wt) (g/mol)	% Calculated (Found)				Molar conductivity $S \cdot cm^2 \cdot mol^{-1}$	
						C%	H%	%N	%M	EtOH	
Ligand = L_1H	Yellow	167	6.5	87	$C_{12}H_{10}Cl_2N_4O_2$ 313.14	46.02 (46.33)	3.21 (3.60)	17.89 (18.00)	–	–	
$[Ni(L_1)_2]\cdot H_2O$	Reddish brown	222	7.5	83	$C_{24}H_{20}N_8O_5Cl_4Ni$ (700.965)	41.12 (41.86)	2.87 (2.99)	15.98 (16.09)	8.37 (8.54)	13.76	
$[Pd(L_1)Cl]\cdot H_2O$	Dark Purple	184	7.5	70	$C_{12}H_{11}N_4O_3Cl_3Pd$ (472.015)	33.03 (33.31)	2.54 (2.60)	12.84 (12.88)	24.39 (24.71)	18.42	
$[Pt(L_1)_2]Cl_2\cdot H_2O$	Yellow red	213	7.5	78	$C_{24}H_{20}N_8O_5Cl_6Pt$ (908.255)	31.74 (31.88)	2.22 (2.29)	12.33 (12.47)	21.47 (21.62)	77.09	

compounds were applied to the monolayer (25, 50, 100, 200, and 400 μg/ml). A metal chelate solution was incubated with monolayer cells for 48 h at 37 °C in 5 % CO_2. ELISA readers (infinite F50, TECAN, Austria) were used to calculate color strength. Standard and control wells were used for each concentration, and vinblastine was used as the control. In the control wells, the percentage of cell viability was 100 %. The absorption values were presented as a percentage of cell viability. Concentrations of each compound were measured three times and mean values and standard deviations (SD) were reported. According to this equation [24], IC_{50} (percentage growth inhibition) = (Control OD−Compound OD/Control OD) × 100.

3. Results and discussion

3.1. Chemistry

By reacting 2-amino-3,4-dimethyl benzoic acid, and 4,5-dichloroimidizol in an alcoholic solution, the tridentate azo dye ligand L_1H was obtained, which was characterized by elemental analysis, FT-IR, UV/vis, NMR, and mass spectroscopy. In addition, the ligand and metal complexes prepared were non-hygroscopic and stable in the air. In ethanol, methanol, DMSO, and DMF, the compounds were soluble. The complexes were measured in EtOH solution for their molar conductances. As a result of the lack of dissociation, Ni(II) complex and Pd(II) complex have non-electrolytic nature, while Pt(II) complex has electrolytic nature. Therefore, the free ligand and its metal complexes may be formulated as shown in Table 1.

3.2. Molar conductivity

Metal complexes in the solution can be studied by measuring conductivity changes. A molar conductance measurement in the EtOH solution of Ni (II) and Pd (II) complexes shows a relatively low value (13.76 and 18.42 $S \cdot cm^2\ mol^{-1}$) which suggests these complexes are non-electrolytes [25]. For Pt(IV) metal complex, EtOH conductivity values are 77.09 $S \cdot cm^2\ mol^{-1}$. Mohr method [26] can be used to determine whether chloride (counter) ions are present or absent. Furthermore, the presence of a white precipitate of Pt(IV) metal complex indicates an electrolytic nature (1:1) electrolyte, and the chloride ion is outside the coordination sphere. The molar conductance of the complexes dissolved in EtOH is shown in Table 1.

3.3. Electronic spectral and magnetic moment studies

The UV-vis spectra of free ligand and metal complexes in EtOH solution are shown in Fig. 1. The free ligand (L_1H) has absorption bands at 389 (25,706 cm^{-1}), 309 nm (32,362 cm^{-1}), and 252 nm (39,682 cm^{-1}), corresponding to the n-π* transition

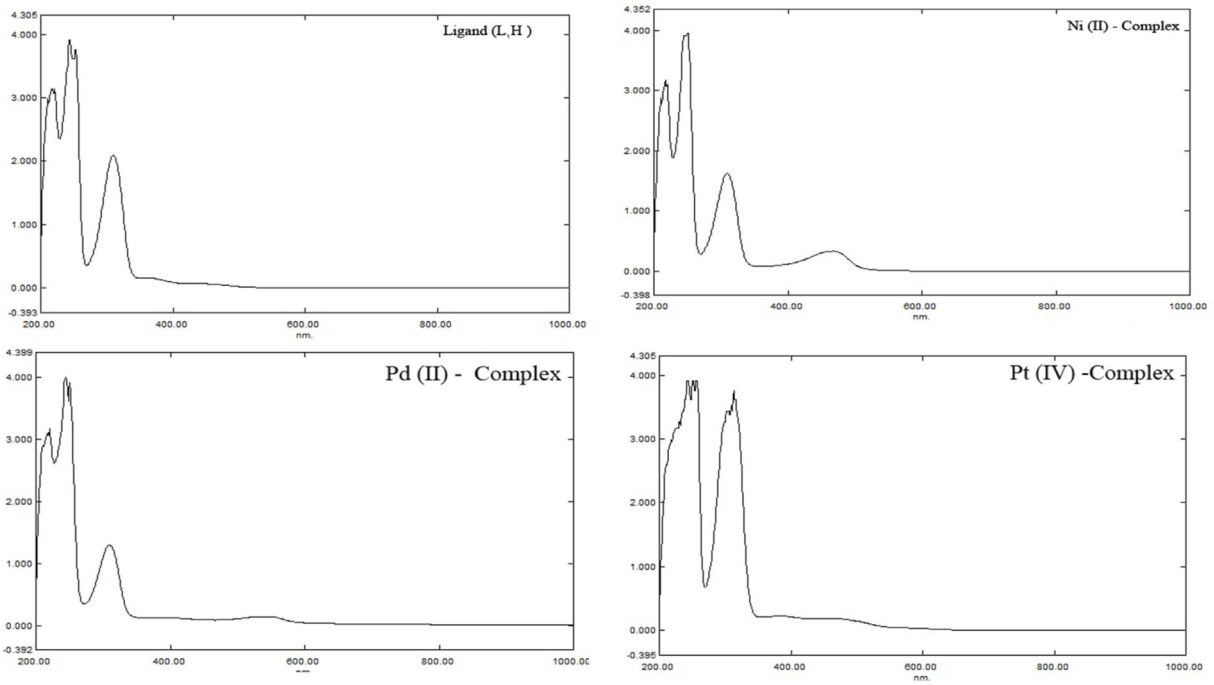

Fig. 1. UV-visible spectra of the ligand ((L_1H) and metal complexes.

of the azomethine group and the azo group of the imidazole molecule, respectively [27]. While π-π* transition corresponds to the aromatic structures or oxygen atom of the −C=O group, as shown in Table 2. The UV−Vis spectrum of Ni(II) complex contained three bands at 468 nm (21,367 cm^{-1}), 309 nm (32,362 cm^{-1}) and 250 nm (40,000 cm^{-1}) due to electronic transitions $^3A_2g \rightarrow {}^3T_2g(F)$ (υ_1), $^3A_2g \rightarrow 3T_1g(F)$($\upsilon_2$) and $^3A_2g \rightarrow {}^3T_1g(p)$($\upsilon_3$), respectively. Magnetic susceptibility indicates that this complex has a paramagnetic moment (μ_{eff} = 1.65 B.M) [28]. The electronic spectrum of the diamagnetic divalent palladium complex showed one absorption peak at 549 nm (18,214 cm^{-1}), belonging to the electronic transmission $^1A_1g \rightarrow {}^1B_1g$, and two peaks at nanometers (cm^{-1}) belonging to the ligand domain, which confirms that the complex above is a square plane, and this is consistent [28]. The electronic spectrum of the diamagnetic platinum (IV) complex showed three absorption peaks belonging to the electronic transmission at the frequency 476 nm (21,008 cm^{-1}), the second at the frequency 431 (23,201 cm^{-1}), and the third at the frequency 348 (25,706 cm^{-1}) belonging to the electronic transitions $^1A_1g \rightarrow {}^1T_1g(F)$ (υ_1), $^1A_1g \rightarrow {}^1T_2g$ (υ_2) and $^1A_1g \rightarrow {}^1Eg$ (υ_3) respectively, and the octahedral geometry formed the complex [21]. Table 6 provides magnetic moment (B.M.) values for metal complexes at room temperature.

3.4. ^1H NMR spectra

^1H NMR spectra have been obtained in DMSO-d_6 at ambient temperature for the azo dye ligand (L_1H) and Pd(II) complex using TMS as an internal reference (500 MHZ) and in comparison with what was reported in the literature [17,29]. Free ligand spectrum displays a signal at (13.8 ppm, 1H, s, 20) due to its carboxylate group, but the loss of the (-COOH) signal from the ^1H NMR spectrum of palladium (II) complex is related to the chelation of metals, which breaks the hydrogen bond (Fig. 2). Further, the ligand shows that the bands observed at (11.66 ppm, 1H, s, 1) ppm and (6.74−7.53 ppm, 2H, m, 13, 14) are

Table 2. Electronic spectra transitions of the ligand ((L_1H) and metal complexes.

Compounds	λ_{max}(nm)	Absorption Bands cm^{-1}	Transitions	μ_{eff} B.M	Geometry	Hybridization
Ligand = L_1H	389	25,706	n—π*	–	–	–
	309	32,362	π —π*			
	252	39,682	π —π*			
$[Ni(L_1)_2]\cdot H_2O$	468	21,367	$^3A_2g \rightarrow {}^3T_2g_{(F)(\upsilon_2)}$	1.65	Octahedral regular	$d^2 sp^3$ (low spin)
	309	32,362	$^3A_2g \rightarrow {}^3T_1g_{(F)(\upsilon_2)}$			
	250	40,000	$^3A_2g \rightarrow {}^3T_1g_{(F)(\upsilon_2)}$			
$[Pd(L_1)Cl]\cdot H_2O$	549	18,214	$^1A_1g \rightarrow {}^1B_1g_{(F)(\upsilon_1)}$	Dia	Square plane (distorted)	dsp^2
$[Pt(L_1)_2]Cl_2\cdot H_2O$	476	21,008	$^1A_1g \rightarrow {}^1T_1g_{(F)(\upsilon_1)}$	Dia	Octahedral (regular)	d^2Sp^3 (low spin)
	431	23,201	$^1A_1g \rightarrow {}^1T_2g_{(F)(\upsilon_2)}$			
	389	25,706	$^1A_1g \rightarrow {}^1E_1g_{(\upsilon_3)}$			

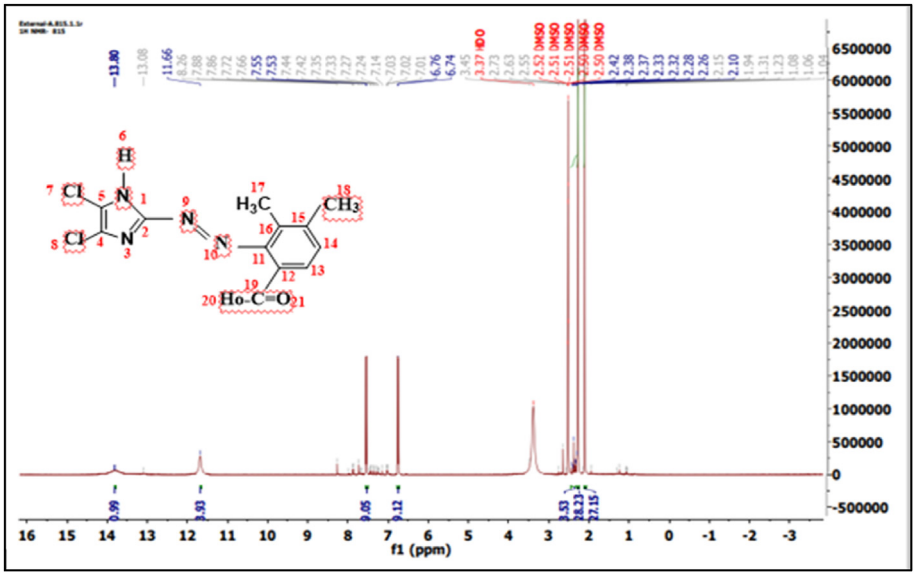

Fig. 2. Proton NMR spectrum of the ligand (L_1H).

assigned to the (NH) group in the imidazole ring, and the aromatic protons, respectively. Also, the ligand exhibited signals of (2.10–2.25 ppm, 3H, s, 17, 18) that belonged to two methyl groups, and a signal at (2.50 ppm, s, solvent proton) returning to the protons of the DMSO-d_6 solvent.

In other complexes, the carboxylate group was deprotonated when there were M – O bonds formed, resulting in the disappearance of ^{1}H NMR signals [17]. ^{1}H NMR spectra of Pd(II)-Complex displayed signals of (12.80 ppm, 1H, s, 1) ppm (δ = 6.37–7.53 ppm, 2H, m, 13, 14) (2.09–2.25 ppm, 3H, s, 17,18) and (2.51 ppm s, solvent proton) that belonged to (NH) group, aromatic protons, methyl groups, and solvent protons, respectively (Fig. 3).

3.5. Mass spectrum

The mass spectra of the synthesized compounds and their main fragments are shown in (Figs. 4 and 5), whereas the fragmentation pattern is shown in (Schemes 2 and 3). A nuclear form of ligand ($C_{12}H_{10}Cl_2N_4O_2$) was detected along with the main signal corresponding to the molecular weight, at *m/z*: 312.3 for the free ligand (M.wt:313.14). For the palladium(II) complex, the signal at *m/z* 473.0 is characteristic of the molecular ion $[M]^+$ could probably correspond to the formula of $C_{12}H_{11}N_4O_3Cl_3Pd$ (M.wt:472.015) [20]. Following are the main signals whose attributes are illustrated in Schemes 2 and 3.

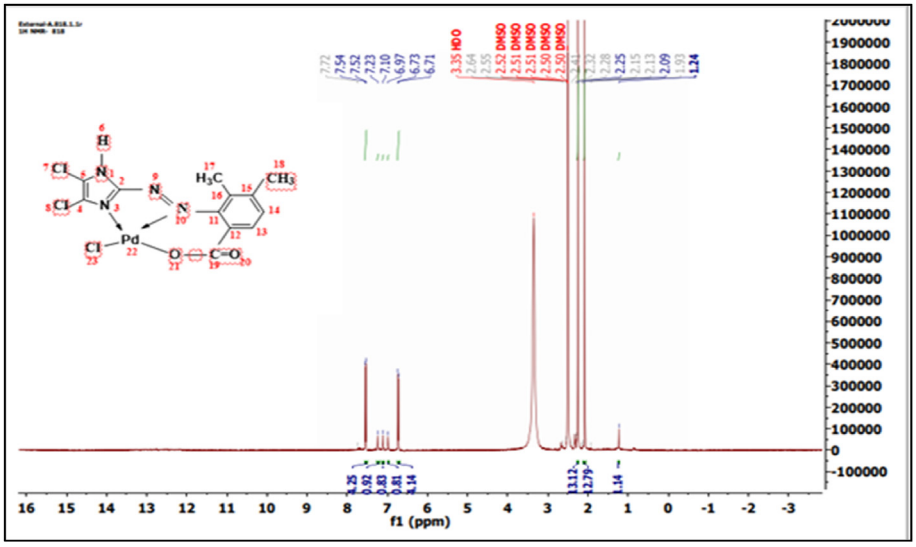

Fig. 3. Proton NMR spectrum of palladium (II) complex.

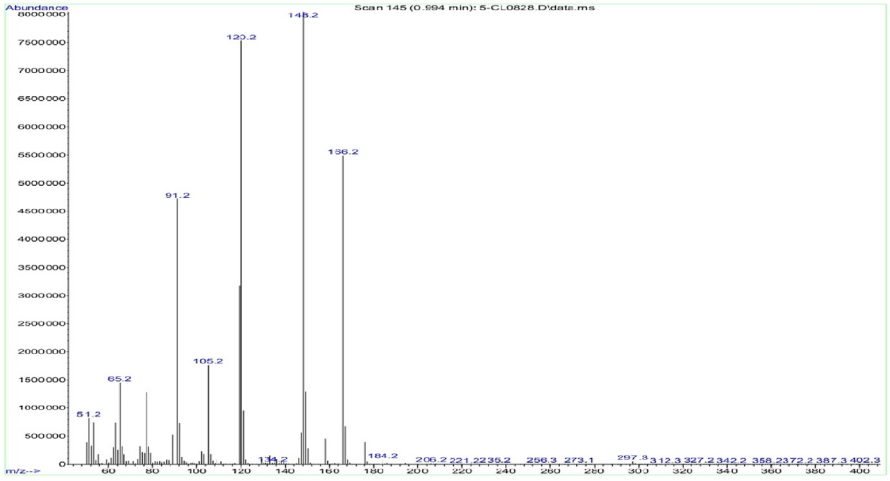

Fig. 4. Mass spectrum of the azo-imidazole ligand (L_1H).

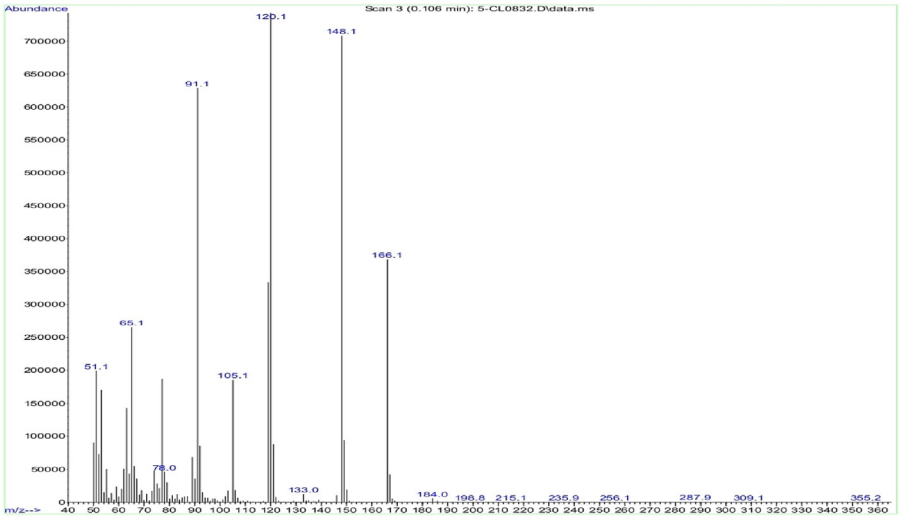

Fig. 5. Mass spectrum of palladium (II) complex.

3.6. Infrared spectra

The FT-IR spectra of the ligand (L_1H) and its metal complexes were recorded in KBr disc between 4000 cm^{-1}–400 cm^{-1} for ligand, Ni(II), Pd(II) and Pt(IV) metal complexes, respectively (Fig. 6). The spectra show that the presence of metal ions has significantly impacted the vibrational modes of the ligand, as indicated by the distinct patterns observed for each of the four samples. Infrared spectra of the ligand (L_1H) revealed a moderate intensity absorption band at frequencies 3350 cm^{-1} owing to stretching vibrations of the carboxyl group (COOH) and a change in intensity and location of this band for all metal complex spectra indicates that bonding through the (COOH) group occurs after the proton has been removed [20]. The appearance of broad FTIR spectra of the complexes Ni(II), Pd(II), and Pt(IV) at 3374, 3345, and 3343 cm^{-1} respectively due to υ(−OH) of water molecules absorbed by the samples or KBr [30]. The ligand and its metal complexes exhibited a medium to weak intensity peak in the region at about 3150, 3158, and 3193 cm^{-1} due to υ(N−H) bond form. The FTIR spectrum of the free ligand has shown a strong υ(C=N) azomethine band at 1630 cm^{-1} however the metal complexes are shifted to higher values at (1637–1644 cm^{-1}) due to the υ(C=N) stretching vibration [31]. Given the frequency shift, it appears that the υ(C=N) bond is coordinated with the metal ion through nitrogen. The peak of the spectrum is observed at (1500, 1515, 1510, and 1512 cm^{-1}), is due to the υ(C=C) stretching of the aromatic ring system of the ligand and Ni(II), Pd(II), and Pt(IV) complexes respectively. In the FT-IR spectra, the ligand and complexes produced several absorption bands within the range (1600-1200 cm^{-1}) caused by vibrations of (N=N), (C=O), and (C-O) bonds. Additionally, the metal complexes provided frequencies for new bands not present in the free ligand spectrum, as they gave bands at frequencies of (5553-586) cm^{-1} and (453–472) cm^{-1}, which are corresponding to the metal-nitrogen (M − N) and metal-oxygen (M − O) [32]. In this way, the coordination occurs through the nitrogen atom of the imidazole ring, the nitrogen atom of the azo bridge group far from the imidazole ring, and the oxygen atom of the carboxyl group after losing its proton [33]. The spectra of the ligand and its complexes are shown in Fig. 6 and Table 3.

In light of the previously described chemical and spectral analyses, it may be possible to suggest a structural formula for chelate complexes as shown in Fig. 7.

3.7. Study of thermal stability

Generally, thermal stability refers to the specific temperature at which a chemical compound begins to decompose along with the release of volatile products, or to the maximum temperature at which the compound can be exposed without causing noticeable changes in nitrogen or oxygen atmospheres [34]. A thermogravimetric analysis (TGA) and differential thermolysis (DTA) technique were employed to study the thermal behavior of azo ligands (L_1H) and metallic complexes under study at temperatures ranging from 40 °C to 800 °C in an inert atmosphere containing nitrogen gas at an average temperature of 20 °C/min^{-1} are shown in Fig. 8 and Table 4. The remaining materials, which

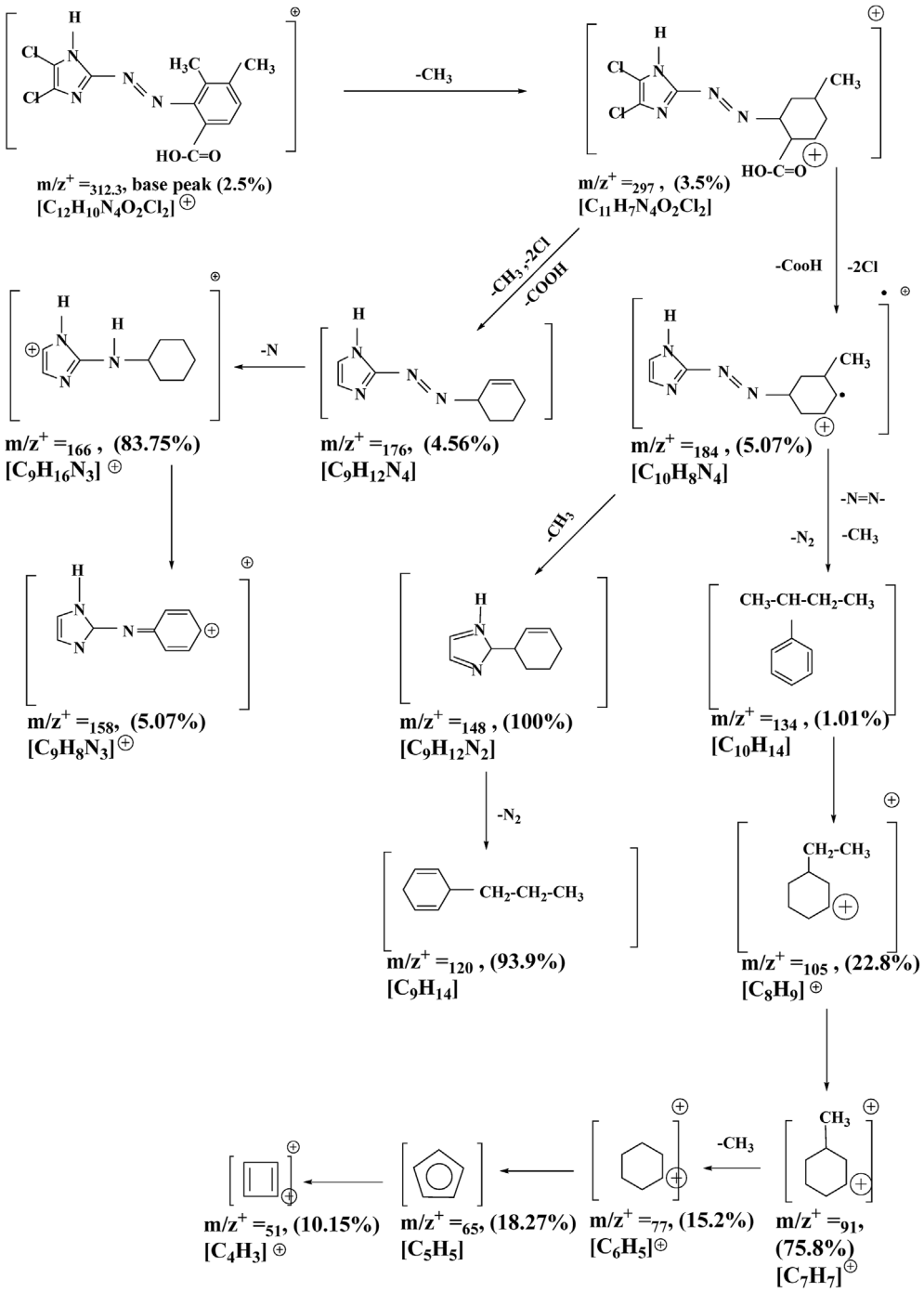

Scheme 2. Proposed mass fractionation pathways for the azo-imidazole ligand (L_1H).

may be formed after thermogravimetric analysis has been completed for the complexes under study, are metal atoms [35].

3.8. Field-emission scanning electron microscope (FESEM) analyzes

The field emission scanning electron microscopy (FE-SEM) of the ligand and metal complexes is used to investigate the surface morphology, shape, and aggregation of particles as well as their distribution. At a cross-sectional distance of 200 nm and a magnification force of 20.00 KX, field emission scanning electron microscopy was used. Fig. 9 shows the FESEM image of the ligand (L_1H), showing that its shape is irregularly sized sheets and that the average size is 92.11 nm. Compared to the nickel complex (II), which had large, oval,

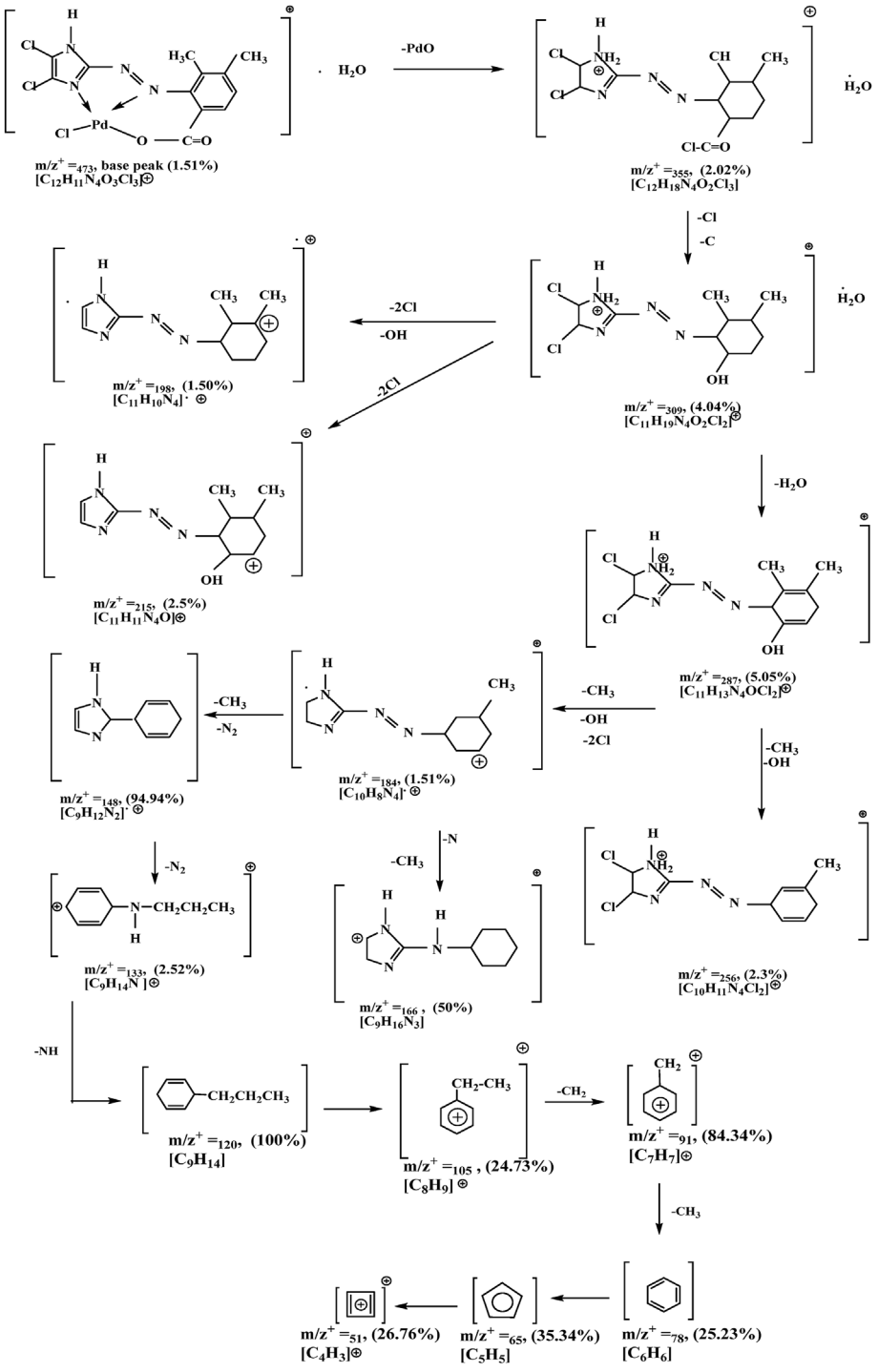

Scheme 3. Proposed mass fractionation pathways for palladium (II) complex.

heterogeneous crystals with an average particle size of 51.2 nm in FESEM analysis. In the FESEM analysis of palladium complex (II) images, heterogeneous crystals were observed and an average particle size of 59.5 nm was determined. While the FESEM image of platinum complex (IV) shows that it is a regular shape and has an average particle size of 81.13 nm. Since metal ions coordinate to donor sites on ligands and their chelates complexes, FESEM micrographs vary considerably [36]. Compound grains are smaller than (100) nm, which is within the nanoscale range. In this case, the surface area can increase effectively and thus enter the (Quantitative effect) to enable the electron to move

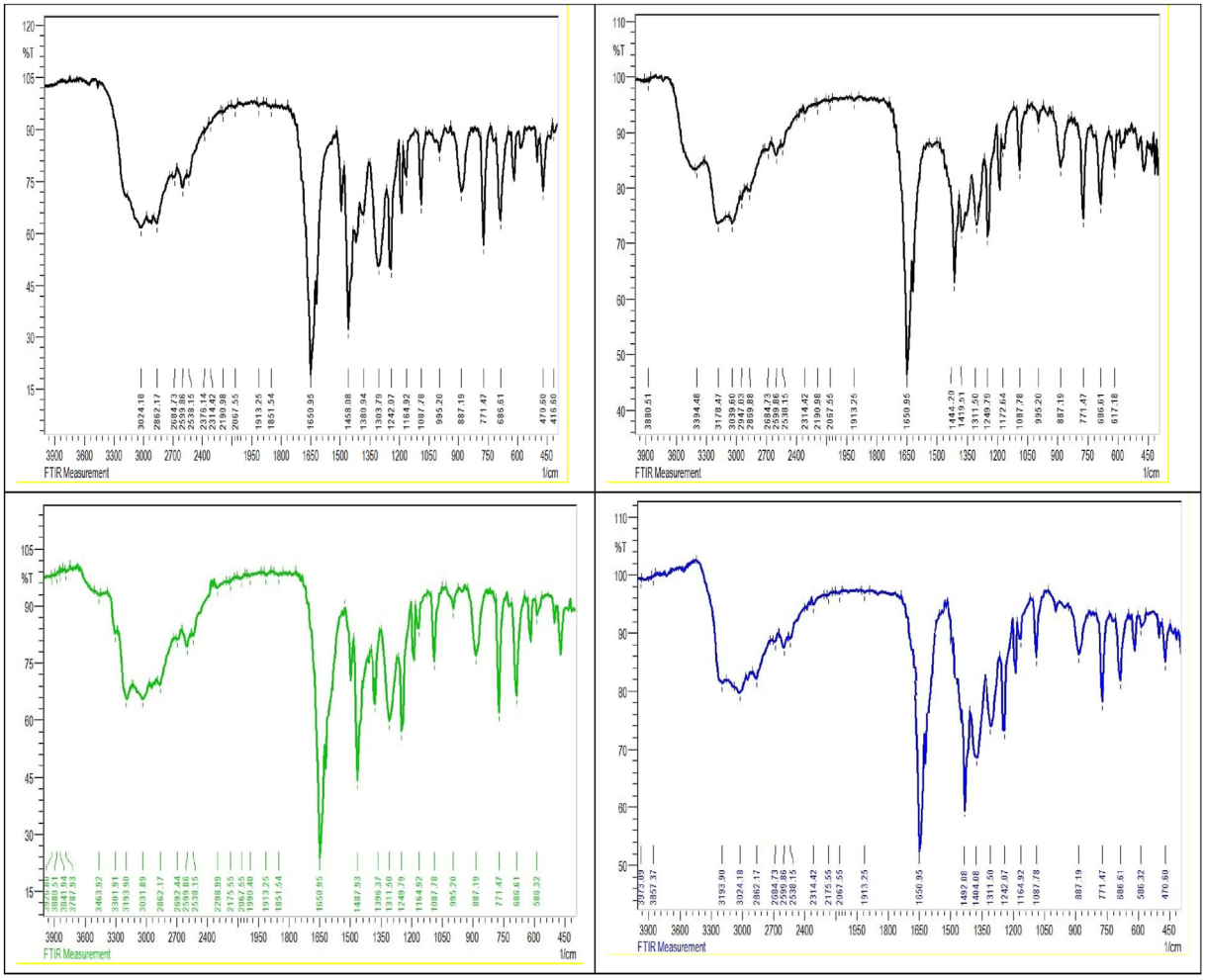

Fig. 6. FT-IR spectrum in KBr solid of ligand and metal complexes.

more freely. Based on the properties of the ligand and its complexes, we were able to study in medicine and the susceptibility of these compounds to inhibit many types of cancer [37].

3.9. X-ray diffraction analysis (XRD)

To determine the crystalline nature and phase purity of the ligand and complexes. The X-ray

Table 3. FT-IR spectra bands of the ligand and their complexes in cm^{-1} units.

Group	Ligand (L_1H)	Ni(II) Complex	Pd(II) Complex	Pt(IV) complex
υ-OH	3350m.br	3374m.br[a]	3345s.br[a]	3343m.br[a]
υ-(NH)	3150m.br	3158s	3193w	3193m
υ-(C=N)	1630m	1640w	1644w	1637m
υ-(C=C)	1500m.br	1515w.br	1510m.br	1512m.br
υ-(C=N)	1458m	1444m	1487s	1492s.br
υ-(N=N)	1650m	1653s	1658s	1652s
υ-(C=O)	1242m	1249s	1248s	1242s
υ-(C-O)	3024w	3039s	3031s	3023m
υ-(C-H)aro	2862m	2869s	2862s	2861s
υ-(C-H) alph	1164s	1172s	1168s	1172s
υ-(C-N=N-C)	1278w	1249 m	1249s	1245s
υ-(M-N)	–	570w	553s	586s
υ-(M-O)	–	470w	453s	472m

S = strong, m = medium, w = weak, br = broad.
[a] (H_2O) outside of sphere coordination.

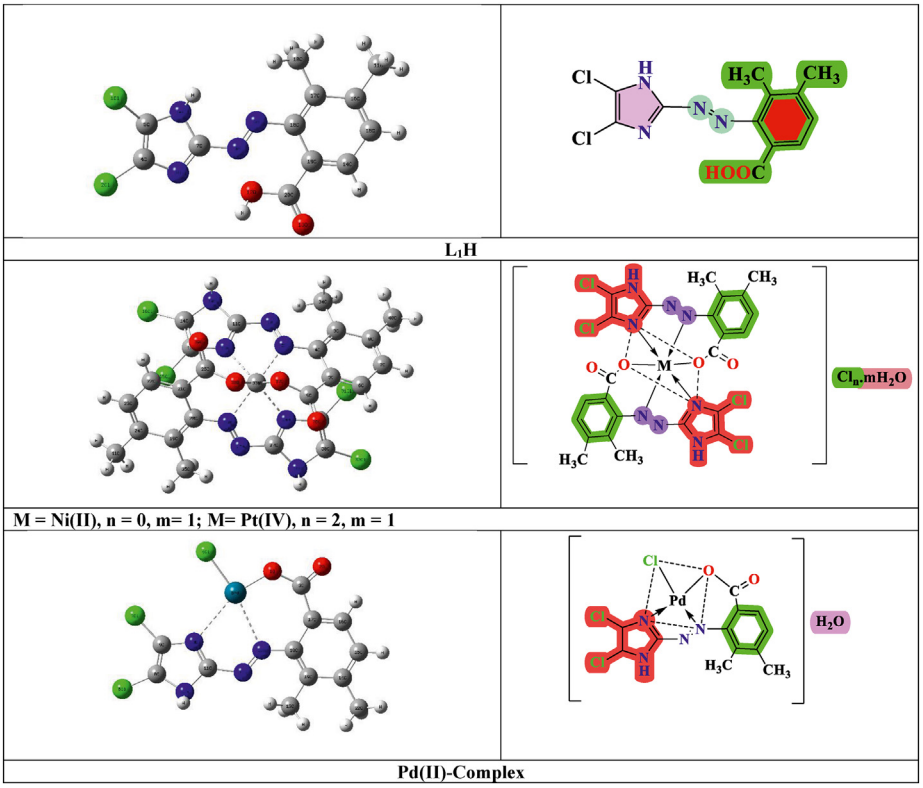

Fig. 7. Creating ligand-chelate complexes according to the suggested formula.

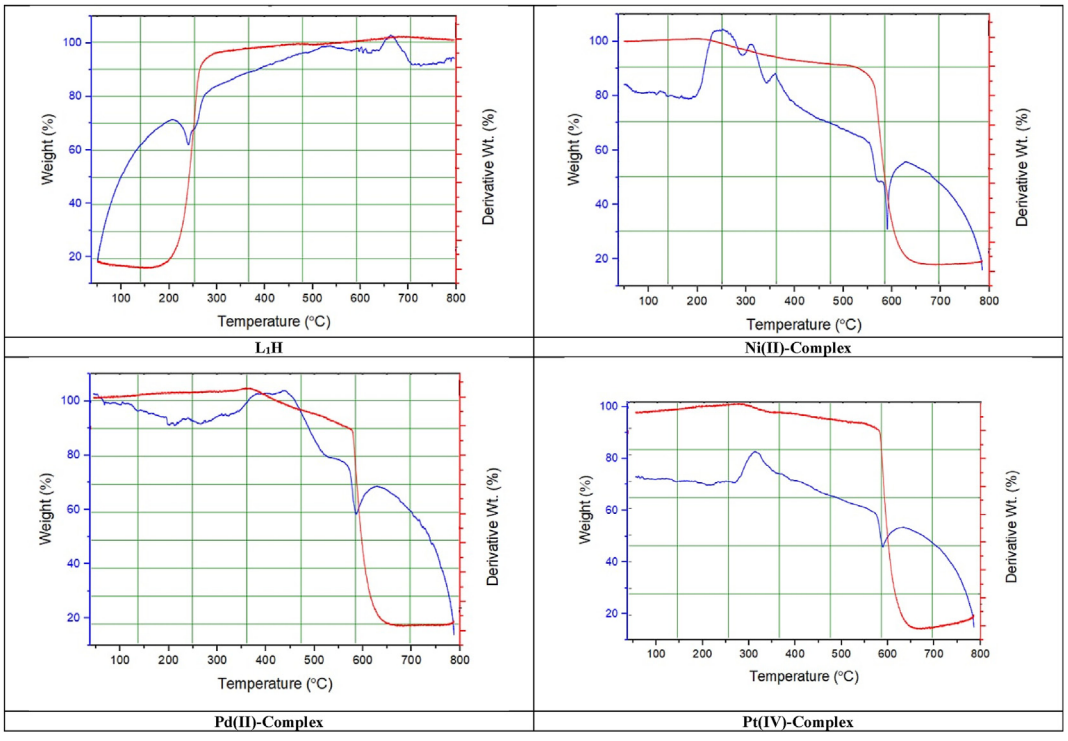

Fig. 8. Thermal decomposition of the free ligand with metal complexes.

Table 4. Thermal decomposition results for azo ligand (L_1H) and their metallic complexes.

Compounds	TG range (°C)	% Estimated		DTG max (°C)	Residue
		Mass loss	Total mass loss		
Ligand = L_1H	50–350	3	79	170	–
	350–700	76		601	
$[Ni(L_1)_2]\cdot H_2O$	200–470	8.49	78.64	250.73	NiO
	470–652	70.15		330.56	
				360.22	
$[Pd(L_1)Cl]\cdot H_2O$	360–470	7.42	92.52	430.27	PdO
	470–660	10.85		580.08	
$[Pt(L_1)_2]Cl_2\cdot H_2O$	280–350	2.51	92.82	315.44	PtO_2
	350–360	90.31		590.71	

diffraction studies (Fig. 10) have been carried out. In the XRD patterns, sharp and intense peaks indicate that the compounds are highly semi-crystalline and pure. Major refluxes were calculated using Bragg's equation [38] and corresponding d-spacing values were determined, where (d) is the spacing between the crystalline levels, (n) is an integer (1,2,3 ..), (λ) is the wavelength of X-ray CuKα = 1.540598 A°, (Θ) is the diffraction angle. Based on the Debye-Scherrer equation [39], the average crystallite size of the particles and their size distributions were determined; where (D) is the average crystallite diameter, (k) is the shape factor (0.891), (λ) is the X-ray wavelength (0.15405 nm), (Θ) is the diffraction angle, and (β) is line broadening at half the maximum intensity (FWHM) in radian of a reported peak. The dislocation density (δ), (the length of dislocation lines per unit volume), can be calculated by using the equation [40]; where is dislocation density, (D) is the average diameter of the crystallite. A microstrain number (ε) was computed based on the following relationship [41]; ε = βCosΘ/4, where (ε) is the microstrain number. Furthermore, we found that the ligand and their metal complexes under study have a granular size lower than 100 nm, indicating that they are within the nanoscale range. While at the same time enhancing according to the results of our previous measurements of field-emission scanning electron microscopy (FESEM) [27,42]. Detailed results of the dislocation density, d-spicing, microstrain, and crystallographic parameters of ligand and chelate complexes are provided in Table 5.

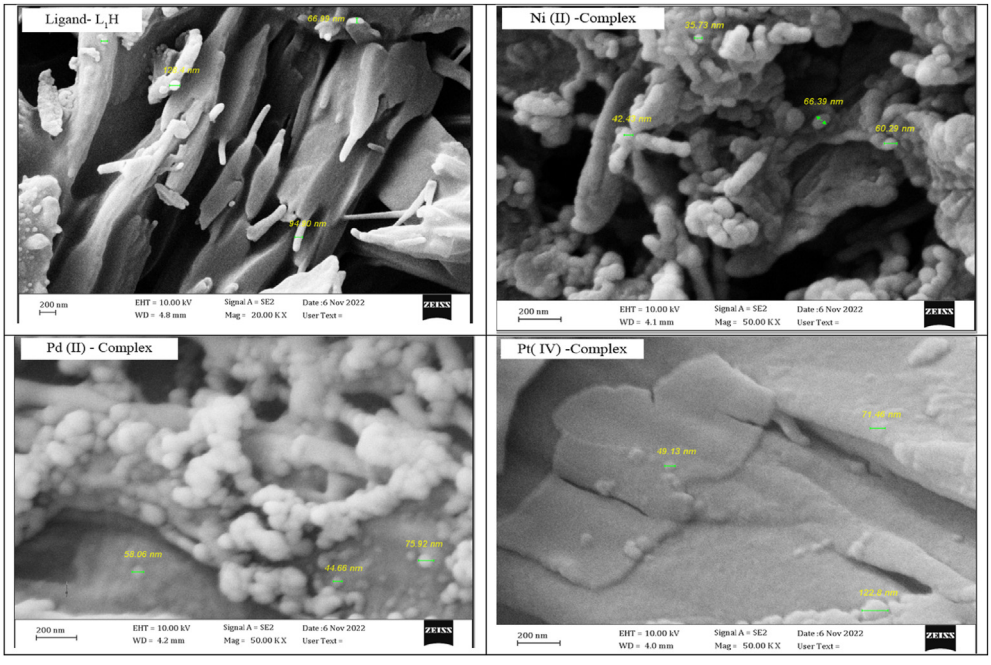

Fig. 9. FESEM images of the ligand (L_1H) and its metallic complexes.

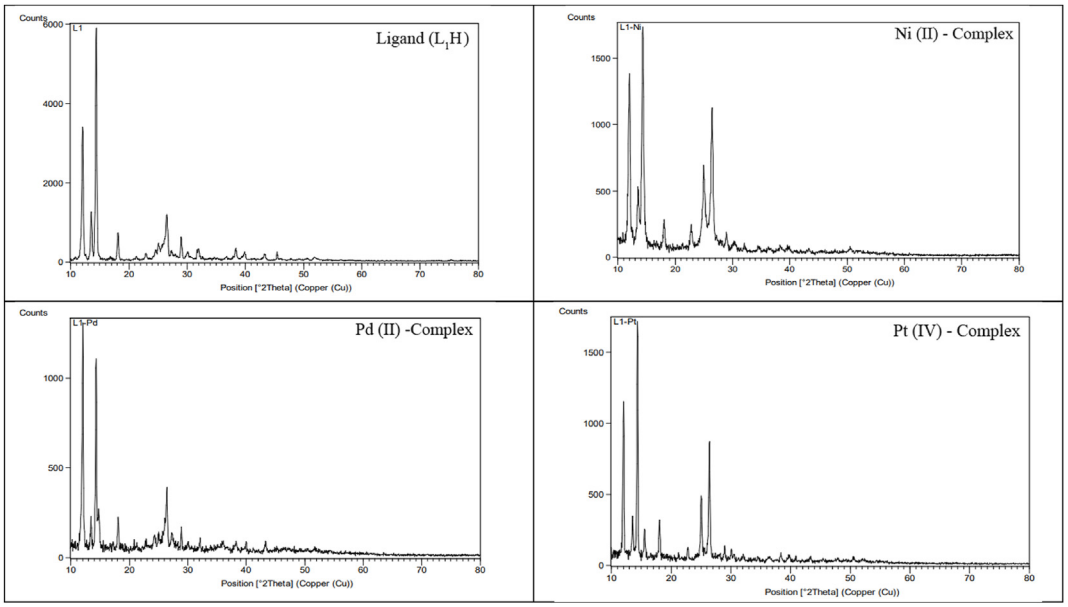

Fig. 10. Represents the X-ray diffraction spectrum of the ligand (L_1H) and its prepared metallic complexes.

3.10. DPPH scavenging activity

The spare electron in 1,1-diphenyl-2-picrylhydrazyl delocalizes over the whole molecule, so it doesn't dimerize like most other free radicals [43]. Compounds that scavenge radicals are identified by identifying hydrogen donors as antioxidants [44]. The antioxidant assays showed that the ligand (L_1H) with its metal complexes, nickel (II), palladium (II), and platinum (IV) under study performed compared with ascorbic acid (Tables 6–9 and Fig. 11). Accordingly, the concentrations of the ligand (L_1H) and its complexes nickel (II), palladium (II), and platinum (IV) were found to have the lowest percentage of inhibition of free radicals (at the lowest concentration of 12.5 mg/ml, the inhibition is (24.46 %), (17.63 %) (17.4 %) (15.78 %), respectively. The highest percentage of free radical inhibition for each ligand (L_1H) at a concentration of 200 mg/ml was (74.07 %), (49.77 %) (75.58 %), and (41.05 %), respectively, as a function of the concentrations of each ligand and its complexes with nickel (II), palladium (II), and platinum (IV).

3.11. Cytotoxic activity (MTT assay)

To compare breast cancer cells MCF-7 and normal cells Hdfn, this study used two types of cell lines. Based on the results, the type and concentration of the compound were important in determining the percentage of cell inhibition. Many researchers agree that this phenomenon is dose-dependent, and is strongly influenced by concentrations and other variables [45–47]. The effect of the ligand on the growth process of breast cancer cells MCF-7 and healthy cells (HdFn) is shown in Table 10 and Fig. 12. The lowest inhibition of breast cancer cell growth was found at (25 μg/ml), while the highest inhibition was found at (400 μg/ml). Furthermore, at a concentration of (50 μg/ml), the lowest percentage of inhibition for healthy cells (HdFn) was found, while at a concentration of 400 μg/ml, the highest percentage was found. Inhibition rates for breast cancer cells were best at 400 μg/ml (57.49 %), while inhibition rates for normal cells were 39.622 % at the same concentration, which is almost a good result, but some modifications are needed to increase the percentage of inhibition. A relationship between the vital activity of MCF-7 breast cancer cells and normal HdFn cells is shown in (Fig. 12). On cancer cell lines, the half-maximum inhibitory concentration (IC_{50}) of the ligand was 0.001 μg/ml, while on normal cells, it was 200.6 μg/ml.

Figure 12 and Table 11 show the effect of the palladium (II) complex on the growth of breast cell lines and normal cells. Based on the obtained results, it was determined that the percentage of remaining live cells of MCF-7 ranged between (75.77 %–96.798 %), while the percentage of normal cells (HdFn) ranged between (85.031 %–96.9 %). Also, the results showed that the lowest percentage of inhibition was for breast cancer cell lines and normal cells (HdFn) at a concentration of 25 μg/ml. In contrast, the highest percentage of inhibition was observed at a concentration of 400 μg/ml for both

Table 5. Parameters of XRD for semi-crystalline compounds.

Compound	Pos. [2Th.]	Height [cts]	FWHM [2Th.]	d-spacing [A°]	Rel. Int. [%]	Crystallite Size D (nm)	Dislocation density $\delta*10^{-3}$ $(nm)^2$	Microstrain $\varepsilon * 10^{-3}$	Average size (nm)
L_1H	12.04	347.5	0.246	7.34809	57.67	33.54	0.88878	10.1743	33.93
	14.37	59.4	0.246	6.16169	100	33.46	0.89298	8.51153	
	18.10	70.1	0.246	4.8988	11.81	33.30	0.90132	6.73564	
	21.289	82.2	0.2952	4.17359	1.37	27.62	1.31047	6.85307	
	27.258	227.9	0.1476	3.27173	3.81	54.63	0.33504	2.65618	
	28.974	582.1	0.246	3.08173	9.74	32.65	0.93768	4.15427	
	30.113	201.6	0.2952	2.96769	3.37	27.14	1.35736	4.78808	
	39.859	194.3	0.246	2.26172	3.25	31.70	0.99455	2.96040	
	43.317	155.6	0.246	2.08884	2.6	31.33	1.01761	2.70297	
Ni(II)-complex	12.0189	954.3	0.1968	7.36381	35.81	41.92	0.56879	8.15706	35.02
	13.5058	384.5	0.1968	6.55627	14.43	41.86	0.57044	7.25199	
	14.3225	264.8	0.1968	6.18422	100	41.83	0.57144	6.83449	
	18.0606	205.2	0.1968	4.91177	7.69	41.63	0.57676	5.40313	
	22.8396	69.42	0.1476	3.8937	2.61	55.10	0.32935	3.18832	
	25.0179	283.2	0.2952	3.55939	10.63	27.44	1.32806	5.80573	
	26.3972	726.3	0.246	3.37646	27.24	32.83	0.92734	4.57687	
	28.8737	166.1	0.1968	3.09225	6.23	40.83	0.59984	3.33551	
	30.2644	32.76	0.5904	2.95325	1.23	13.56	5.43330	9.52618	
	39.6246	21.68	0.5904	2.27455	0.81	13.22	5.72018	7.15059	
Pd(II)-complex	13.4613	147.7	0.1968	6.57785	11.57	41.87	0.57039	7.27618	35.9
	14.7595	176.9	0.1968	6.00206	13.86	41.81	0.57199	6.62998	
	18.1004	163.5	0.1968	4.90106	12.81	41.63	0.57683	5.39105	
	21.035	18.5	0.7872	4.22349	1.45	10.36	9.31121	18.5010	
	24.3035	73.18	0.2952	3.66238	5.73	27.47	1.32444	5.98186	
	27.2811	80.91	0.1968	3.26904	6.34	40.97	0.59569	3.53848	
	32.073	66.58	0.1476	2.79072	5.22	54.02	0.34258	2.24059	
	38.227	45.48	0.2952	2.35444	3.56	26.55	1.41777	3.71684	
	43.2921	56.69	0.1968	2.08999	4.44	39.18	0.65116	2.16375	
Pt(IV)-complex	11.9946	105.6	0.246	7.37867	58.83	33.54	0.88870	10.2171	26.47
	14.344	170.4	0.1968	6.175	100	41.83	0.57146	6.82414	
	22.7857	68.89	0.1968	3.90279	4.03	41.33	0.58540	4.26143	
	26.3957	850.2	0.246	3.37665	49.74	32.83	0.92734	4.57714	
	30.0866	74.81	0.1968	2.9703	4.38	40.71	0.60319	3.19505	
	36.4312	21.49	0.7872	2.46626	1.26	10.01	9.97574	10.4374	
	39.782	34.73	0.492	2.26591	2.03	15.85	3.97629	5.93325	
	40.8592	26.03	0.2952	2.20863	1.52	26.33	1.44137	3.45800	
	47.8249	17.5	0.5904	1.90195	1.02	12.84	6.05845	5.80990	
	52.1457	15.67	0.7872	1.75407	0.92	9.467	11.1560	7.01973	

Table 6. Comparison of mean values between L_1H and ascorbic acid.

Concentrations $\mu g\ mL^{-1}$	Vit. C			L_1H			Adjusted P Value
	Mean	SD	SEM	Mean	SD	SEM	
200	79.98	2.692	1.554	74.07	4.783	2.762	0.4823
100	72.18	3.307	1.909	63.85	3.549	2.049	0.1604
50	54.48	2.412	1.393	52.2	3.713	2.144	0.9799
25	40.43	7.081	4.088	40.55	4.263	2.461	>0.9999
12.5	17.63	7.196	4.155	24.46	2.938	1.696	0.332

SD: Standard Deviation.

Table 7. Comparison of mean values between L1Ni and ascorbic acid.

Concentrations $\mu g\ mL^{-1}$	Vit. C			L1Ni			Adjusted P Value
	Mean	SD	SEM	Mean	SD	SEM	
200	79.98	2.692	1.554	49.77	10.67	6.158	<0.0001
100	72.18	3.307	1.909	42.79	1.794	1.036	<0.0001
50	54.48	2.412	1.393	32.52	1.446	0.8346	0.0003
25	40.43	7.081	4.088	18.98	4.703	2.715	0.0004
12.5	17.63	7.196	4.155	17.63	3.506	2.024	>0.9999

SD: Standard Deviation.

Table 8. Comparison of mean values between L1Pt and ascorbic acid.

Concentrations μg mL^{-1}	Vit. C			L_1Pt			Adjusted P Value
	Mean	SD	SEM	Mean	SD	SEM	
200	79.98	2.692	1.554	41.05	2.655	1.533	<0.0001
100	72.18	3.307	1.909	37.24	1.27	0.7331	<0.0001
50	54.48	2.412	1.393	13.85	2.8	1.617	<0.0001
25	40.43	7.081	4.088	16.9	5.315	3.069	<0.0001
12.5	17.63	7.196	4.155	15.78	0.9351	0.5399	0.9884

SD: Standard Deviation.

Table 9. Comparison of mean values between L1Pd and ascorbic acid.

Concentrations μg mL^{-1}	Vit. C			L_1Pd			Adjusted P Value
	Mean	SD	SEM	Mean	SD	SEM	
200	79.98	2.692	1.554	75.58	5.843	3.373	0.7884
100	72.18	3.307	1.909	63.43	3.614	2.086	0.1595
50	54.48	2.412	1.393	54.48	2.695	1.556	>0.9999
25	40.43	7.081	4.088	36.96	4.945	2.855	0.9069
12.5	17.63	7.196	4.155	17.4	4.207	2.429	>0.9999

SD: Standard Deviation.

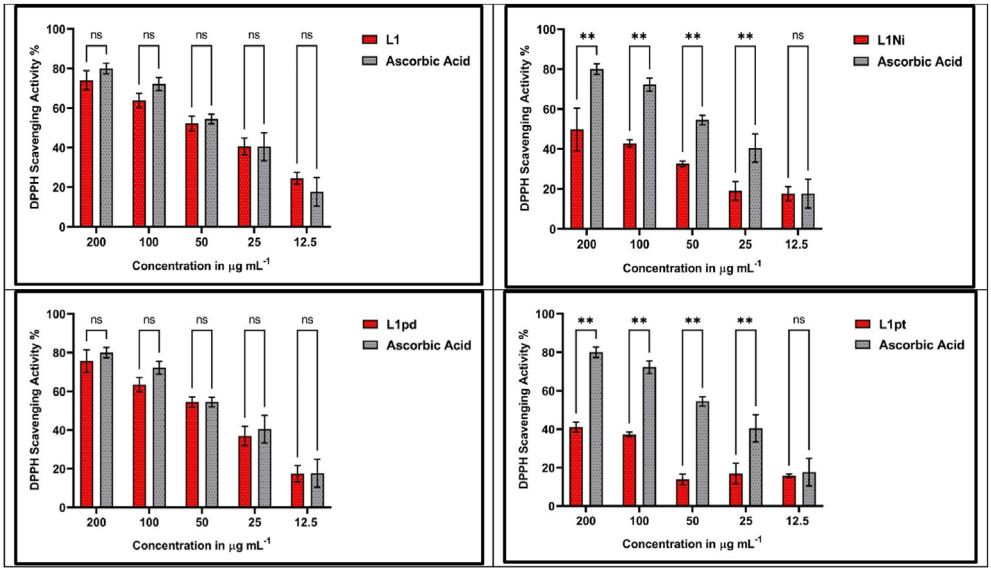

Fig. 11. Comparison between L_1H, Ni(II), Pd(II), Pt(IV) metal complexes and ascorbic acid at different concentrations in DPPH scavenging activity %. There was no significant difference between compounds and ascorbic acid. Data are expressed as means ± SD.

Table 10. Comparison of the effect of the ligand (L_1H) on the cells of the breast cancer line MCF-7 with a normal cell line using MTT for 48 h at 37 °C.

ligand (L_1H)				
Con. (μg·mL^{-1})	Cancer line cells of MCF-7		Normal line cells HdFn	
	Mean	SD	Mean	SD
25	92.091	5.78	95.216	0.82
50	71.142	0.82	95.33	1.18
100	62.731	3.06	93.5	2.1
200	49.807	5.20	77.08	5.5
400	42.51	2.56	60.378	0.8

together. The inhibition rate with MCF-7 breast cancer cells (MCF-7) of palladium (II) complex at 400 μg/ml was 24.23 %. Normal cell line (HdFn) inhibition at the same concentration above was 14.969 %, which is an excellent result and indicates the potential for using this complex as a treatment for breast cancer. Compared with healthy cells (HdFn), it showed the best ratio of inhibiting cancer cell growth. Palladium (II) complex half-inhibition concentration fifty (IC_{50}) with MCF-7 breast cancer cells was 272.9 μg/ml, while for normal cells, it was 125.6 μg/ml.

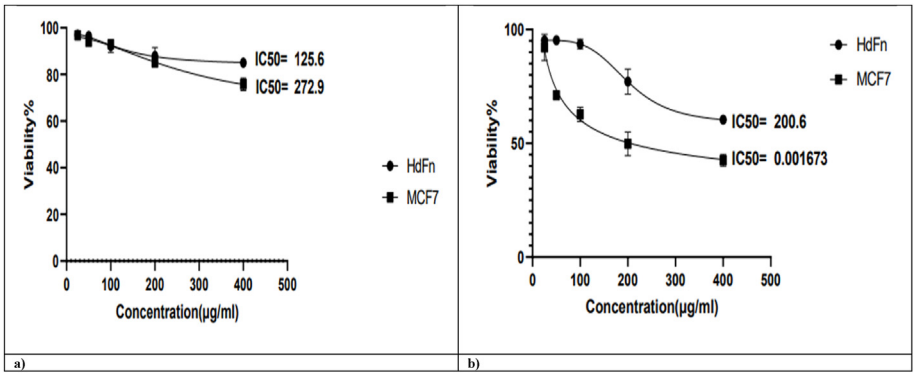

Fig. 12. Graphical representation of the anticancer activity of a ligand b Pd(II) complex: IC_{50} against(MCF-7) cancer cells and normal cells (Hdfn). The data shown are the mean standard error of at least three independent experiments.

Table 11. Comparison of the effect of palladium complex [Pd(L_1) Cl]·H_2O) with ligand ((L_1H) on breast cancer cells MCF7 with normal cell lines using MTT assay for 48 h at 37 °C.

Con. ($\mu g \cdot mL^{-1}$)	[Pd(L_1) Cl]·H_2O			
	Cancer line cells of MCF7		Normal line cells HdFn	
	Mean	SD	Mean	SD
25	96.798	0.93	96.9	1.14
50	94.05	1.38	96.48	1.29
100	92.93	0.83	92.207	2.7
200	85.108	1.2	87.92	3.57
400	75.77	2.6	85.031	1.03

4. Conclusion

In this paper, we describe have prepared a series of three novel metals complexes, Ni(II), Pd(II), and Pt(IV), with new azo dye ligand derived by the diazotization and coupling reactions of 2-amino-3,4-dimethyl benzoic acid and 4,5-dichloroimidizol. A variety of physicochemical and spectrochemical techniques were used to characterize the synthesized compounds. According to ^{1}H-NMR and FT-IR, the coordination sites are azomethine nitrogen, azo nitrogen, and carboxylic oxygen. In addition, Ni(II), and Pt(IV) metal complexes have 2:1 (ligand:metal) stoichiometry, whereas Pd(II) has 1:1 (ligand:metal). In the DPPH assay, three complexes of the ligand were evaluated for antioxidant activity. Furthermore, the maximum antioxidant capacity was found to be in the Pd(II) complex, followed by the Ni(II) complex. In vitro cytotoxicity studies by MTT assay showed that the ligand and Pd(II) complex displayed significant cytotoxic activity against MCF-7 and normal cells (Hdfn).

Funding

Self-funding.

References

[1] Ismael Mohamed, Abdou Aly, Abdel-Mawgoud A-M. Synthesis, characterization, modeling, and antimicrobial activity of FeIII, CoII, NiII, CuII, and ZnII complexes based on trisubstituted imidazole ligand. Z Anorg Allg Chem 2018; 644(20):1203–14.
[2] Kumari S, Maddeboina K, Bachu RD, Boddu SHS, Trippier PC, Tiwari AK. Pivotal role of nitrogen heterocycles in Alzheimer's disease drug discovery. Drug Discov Today 2022 Oct;27(10):103322. https://doi.org/10.1016/j.drudis.2022.07.007. Epub 2022 Jul 19. PMID: 35868626.
[3] Grimmett M Ross. Imidazole and benzimidazole synthesis. Academic press; 1997.
[4] Vasava Mahesh S, Bhoi Manoj N, Rathwa Sanjay K, Jethava Divya J, Acharya Prachi T, Patel Dhaval B, et al. Benzimidazole: a milestone in the field of medicinal chemistry. Mini Rev Med Chem 2020;20(7):532–65.
[5] Alkahtani Hamad M, Abbas Abdullahi Y, Wang Shudong. Synthesis and biological evaluation of benzo [d] imidazole derivatives as potential anti-cancer agents. Bioorg Med Chem Lett 2012;22(3):1317–21.
[6] Fernando C Torres, Eugenia Garcia-Rubino M, Lozano-Lopez Cesar, Kawano Daniel F, Eifler-Lima Vera L, Poser Gilsane L von, et al. Imidazoles and benzimidazoles as tubulin-modulators for anti-cancer therapy. Curr Med Chem 2015;22(11):1312–23.
[7] Narasimhan Balasubramanian, Sharma Deepika, Kumar Pradeep. Biological importance of imidazole nucleus in the new millennium. Med Chem Res 2011;20:1119–40.
[8] Ayaz Furkan, Yetkin Derya, Yüzer Abdulcelil, Demircioğlu Kübra, Ince Mine. Non-canonical anti-cancer, anti-metastatic, anti-angiogenic and immunomodulatory PDT potentials of water soluble phthalocyanine derivatives with imidazole groups and their intracellular mechanism of action. Photodiagnosis Photodyn Ther 2022;39:103035.
[9] Vijesh AM, Isloor Arun M, Telkar Sandeep, Arulmoli T, Fun Hoong-Kun. Molecular docking studies of some new imidazole derivatives for antimicrobial properties. Arab J Chem 2013;6(2):197–204.
[10] Dahiya Rajiv. Synthesis, characterization and antimicrobial studies on some newer imidazole analogs. Sci Pharm 2008; 76(2):217–40.
[11] Mohammed AL, Salih Hadi Kadhim. Preparation and identification of Co (Ll), Ni (Ll), Cu (Ll) complexes with a new 4-(4-(1-(2-Hydroxyl phenyl) amino) Ethyl phenyl) azo-2, 6-dimethyl phenol ligand. HIV Nursing 2022;22(2):878–82.
[12] Morshedi Dina, Mohammadi Zeinab, Boojar Masoud Mashhadi Akbar, Aliakbari Farhang. Using protein nanofibrils to remove azo dyes from aqueous solution by the

coagulation process. Colloids Surf B Biointerfaces 2013;112: 245−54.
[13] Aljamali Nagham Mahmood, Hassen Huda Sabah. Review on azo-compounds and their applications. J Catal Catalys 2021;8(2):8−16p.
[14] Beharry Andrew A, Andrew Woolley G. Azobenzene photoswitches for biomolecules. Chem Soc Rev 2011;40(8): 4422−37.
[15] Hasan Rawaa Ch, Karam Faiq F, Baqir Sadiq J. Synthesis and characterization of a novel organic reagent and its complexes with Cu (||), Cr (|||), Co (|||) and Fe (|||) metal. IOP Conf Ser Earth Environ Sci 2022;1029(1):012027. IOP Publishing.
[16] Moradi Omid, Pudineh Afshin, Sedaghat Sajjad. Synthesis and characterization Agar/GO/ZnO NPs nanocomposite for removal of methylene blue and methyl orange as azo dyes from food industrial effluents. Food Chem Toxicol 2022;169: 113412.
[17] Al-Adilee Khalid, Hussein AK Kyhoiesh. Preparation and identification of some metal complexes with new heterocyclic azo dye ligand 2-[2−-(1-Hydroxy-4-Chloro phenyl) azo]-imidazole and their spectral and thermal studies. J Mol Struct 2017;1137:160−78.
[18] Abd Al-Sadda HK, Al-Hussainawy MK, Kyhoiesh HAK. Synthesis, spectral characterization and biological activity of 2-[2-(1-amino-1, 5-dinitrophenyl) azo]-imidazole. J Glob Pharma Technol 2019;11(7):165−74.
[19] Al-Adilee Khalid J, Kyhoiesh Hussein Ali Kadhim, Taher Ali M. Synthesis, characterization, biological studies, molecular docking and theoretical calculation of some transition metal complexes with new azo dye 2-[2′-(6-methoxybenzothiazolyl) azo]-3-methyl-4-nitrophenol. Results Chem 2022;4:100500.
[20] Kyhoiesh Hussein Ali Kadhim, Al-Adilee Khalid J. Synthesis, spectral characterization and biological activities of Ag (I), Pt (IV) and Au (III) complexes with novel azo dye ligand (N, N, O) derived from 2-amino-6-methoxy benzothiazole. Chem Paper 2022:1−34.
[21] Kyhoiesh Hussein Ali Kadhim, Al-Adilee Khalid J. Synthesis, spectral characterization, antimicrobial evaluation studies and cytotoxic activity of some transition metal complexes with tridentate (N, N, O) donor azo dye ligand. Results Chem 2021;3:100245.
[22] Zhu Kexue, Zhou Huiming, Qian Haifeng. Antioxidant and free radical-scavenging activities of wheat germ protein hydrolysates (WGPH) prepared with alcalase. Process Biochem 2006;41(6):1296−302.
[23] Finn GJ, Creaven B, Egan DA. Study of the in vitro cytotoxic potential of natural and synthetic coumarin derivatives using human normal and neoplastic skin cell lines. Melanoma Res 2001;11(5):461−7.
[24] Kostova Irena. Synthetic and natural coumarins as cytotoxic agents. Curr Med Chem Anti Cancer Agents 2005;5(1):29−46.
[25] Waheeb Azal Shakir, Kyhoiesh Hussein Ali Kadhim, Salman Abbas Washeel, Al-Adilee Khalid J, Kadhim Mustafa M. Metal complexes of a new azo ligand 2-[2′-(5-nitrothiazolyl) azo]-4-methoxyphenol (NTAMP): synthesis, spectral characterization, and theoretical calculation. Inorg Chem Commun 2022;138:109267.
[26] Azmat R, Masood S, Ahmed T, Ahmed W. Application of Mohr's method for the determination of chloride in plant tissue extracts using the conductometric titration. Pak J Chem 2021;11(1−4):28−32.
[27] Kyhoiesh Hussein Ali Kadhim, Al-Hussainawy Mohammed K, Waheeb Azal Shakir, Al-Adilee Khalid J. Synthesis, spectral characterization, lethal dose (LD50) and acute toxicity studies of 1, 4-Bis (imidazolylazo) benzene (BIAB). Heliyon 2021;7(9):e07969.
[28] Jaber Sudad A, Hussein AK Kyhoiesh, Jawad Sajjad H. Synthesis, characterization and biological activity studies of cadmium (II) complex derived from azo ligand 2-[2↖-(5-bromo Thiazolyl) azo]-5-dimethyl amino benzoic acid. J Phys Conf 2021;1818(1):012013. IOP Publishing.
[29] Kyhoiesh Hussein Ali Kadhim, Al-Hussainawy Mohammed K, Haider Radhi Saud. Synthesis and characterization of polyacrylamide/crotonic acid and its composites with carbon nanotube and Rhodamine B. AIP Conf Proc 2022;2398(1): 030018. AIP Publishing LLC.
[30] Al-Hussainawy Mohammed K, Mehdi Zaman Sahb, Jasim Khawla K, Abbas Alshamsi Hassan, Saud Haider R, Hussein Ali Kadhim Kyhoiesh. A single rapid route synthesis of magnetite/chitosan nanocomposite: competitive study. Results Chem 2022;4:100567.
[31] Bandyopadhyay Anasuya, Higuchi Masayoshi. From metal complexes to metallosupramolecular polymers via polycondensation: synthesis, structure and electrochromic properties of Co (III)-and Fe (III)-based metallosupramolecular polymers with aromatic azo ligands. Eur Polym J 2013;49(6):1688−97.
[32] Masoud Mamdouh S, Hemdan Sokaina S, Elsamra Rehab MI. Synthesis, ligating properties, thermal behavior, computational and biological studies of some azo-transition metal complexes. J Inorg Organomet Polym Mater 2022:1−18.
[33] Agarwal Pratibha, Kumar Akhilesh, Verma Indresh, Khanum Ghazala, Siddiqui Nazia, Choquesillo-Lazarte Duane, et al. Dinuclear phenoxo-bridged nickel (II) and copper (II) complexes of phenolate-based tripodal ligand: theoretical and experimental insights. Polycycl Aromat Comp 2023:1−20.
[34] Chang Hua, Pei Jane Huang. Thermal decomposition of CaC2O4⊙ H2O studied by thermo-Raman spectroscopy with TGA/DTA. Anal Chem 1997;69(8):1485−91.
[35] Biamino S, Badini C. Combustion synthesis of lanthanum chromite starting from water solutions: investigation of process mechanism by DTA−TGA−MS. J Eur Ceram Soc 2004;24(10−11):3021−34.
[36] Li Zhanfeng, Dong Jun, Wang Lun, Zhang Yongqiang, Zhuang Tingting, Wang Huiqi, et al. A power-triggered preparation strategy of nano-structured inorganics: sonosynthesis. Nanoscale Adv 2021;3(9):2423−47.
[37] Bai Xiao, More Karren, Rouleau Christopher M, Rabiei Afsaneh. Functionally graded hydroxyapatite coatings doped with antibacterial components. Acta Biomater 2010; 6(6):2264−73.
[38] Wachid Frischa M, Perkasa Adhi Y, Prasetya Fandi A, Rosyidah Nurul, Darminto. Synthesis and characterization of nanocrystalline graphite from coconut shell with heating process. AIP Conf Proc 2014;1586(1):202−6. American Institute of Physics.
[39] Singh Jitendra Pal, Won Sung Ok, Lim Weon Cheol, Lee Ik-Jae, Chae KH. Electronic structure studies of chemically synthesized MgFe2O4 nanoparticles. J Mol Struct 2016;1108: 444−50.
[40] Shaaban Essam R, Afify N, Atef El-Taher. Effect of film thickness on microstructure parameters and optical constants of CdTe thin films. J Alloys Compd 2009;482(1−2):400−4.
[41] Basak Munmun, Rahman Md Lutfor, Ahmed Md Farid, Biswas Bristy, Sharmin Nahid. The use of X-ray diffraction peak profile analysis to determine the structural parameters of cobalt ferrite nanoparticles using Debye-Scherrer, Williamson-Hall, Halder-Wagner and Size-strain plot: different precipitating agent approach. J Alloys Compd 2022; 895:162694.
[42] Tatarchuk Tetiana, Myslin Mariana, Mironyuk Ivan, Bououdina Mohamed, Pędziwiatr Antoni T, Gargula Renata, et al. Synthesis, morphology, crystallite size and adsorption properties of nanostructured Mg−Zn ferrites with enhanced porous structure. J Alloys Compd 2020;819:152945.
[43] Locatelli Monica, Gindro Roberto, Travaglia Fabiano, Coïsson Jean-Daniel, Rinaldi Maurizio, Arlorio Marco. Study of the DPPH-scavenging activity: development of a free software for the correct interpretation of data. Food Chem 2009;114(3):889−97.
[44] Marinova Gabriela, Batchvarov Valentin. Evaluation of the methods for determination of the free radical scavenging activity by DPPH. Bulg J Agric Sci 2011;17(1):11−24.
[45] Han Junkyu, Talorete Terence PN, Yamada Parida, Isoda Hiroko. Anti-proliferative and apoptotic effects of

oleuropein and hydroxytyrosol on human breast cancer MCF-7 cells. Cytotechnology 2009;59:45−53.
[46] Yu Zengli, Zhang Lishi, Wu Desheng, Liu Fuyun. Anti-apoptotic action of zearalenone in MCF-7 cells. Ecotoxicol Environ Saf 2005;62(3):441−6.
[47] Chuthapisith Suebwong, Layfield Robert, Kerr Ian D, Hughes Catherine, Eremin Oleg. Proteomic profiling of MCF-7 breast cancer cells with chemoresistance to different types of anti-cancer drugs. Int J Oncol 2007;30(6): 1545−51.